Inorg. Chem. **2006**, *45*, 2812–2823

Solution and Solid-State Properties of Luminescent M–M Bond-Containing Coordination/Organometallic Polymers Using the RNC-M_2(dppm)$_2$-CNR Building Blocks (M = Pd, Pt; R = Aryl, Alkyl)

Jean-François Bérubé,[1a] Karl Gagnon,[1a] Daniel Fortin,[1a] Andreas Decken,[1b] and Pierre D. Harvey*[,1a]

Département de Chimie, Université de Sherbrooke, Sherbrooke, PQ, Canada J1K 2R1, and Department of Chemistry, University of New Brunswick, Fredericton, NB, Canada E3B 6E2

Received June 12, 2005

Two families of organometallic polymers built upon the bimetallic $M_2(dppm)_2L_2^{2+}$ fragments (M = Pd, Pt; dppm = bis(diphenylphosphino)methane, L = 1,4-diisocyano-2,3,5,6-tetramethylbenzene (diiso), 1,8-diisocyano-p-menthane (dmb), 1-isocyano-2,6-dimethylbenzene, 1-isocyano-4-isopropylbenzene, and *tert*-butylisocyanide) were synthesized and fully characterized (^{1}H and ^{31}P NMR, X-ray crystallography (model compounds), IR, Raman, chem. anal., TGA, DSC, powder XRD, ^{31}P NMR T_1 and NOE, light scattering, and conductivity measurements). Evidence for polymers in the solid state is provided from the swelling of the polymers upon dissolution and the formation of stand-alone films. However, these species become small oligomers when dissolved. The materials are luminescent in the solid state at 298 and 77 K and in PrCN solution at 77 K. These emissions result from triplet ^{3}(dσdσ^*) states despite the presence of low-lying π–π^* MO levels according to DFT calculations for the aryl isocyanide model compounds. The emission band maxima are located between 640 and 750 nm and exhibit lifetimes of 3–6 ns for the Pd species and 3–4 μs for the Pt analogues in PrCN solution at 77 K. No evidence of intramolecular excitonic photoprocesses was found in any of the polymers.

Introduction

The design of organometallic and coordination polymers where the metallic fragment is incorporated in the backbone has become a field of growing interest in recent years.[2] Among these new materials, the Pd- and Pt-isocyanide-containing oligomers and polymers form an interesting family of conjugated compounds, investigated for their optical, luminescence, and conductivity properties.[2i] Well-characterized examples of the incorporation of M−M bonds in the backbone of organometallic/coordination polymers are relatively rare,[3,4] and most of them are nonconjugated. The incorporation of Pt−Pt bonds in isocyanide-containing polymers was first introduced by Puddephatt and co-workers using bridging "C≡NArN≡C" ligands where Ar = *p*-C_6H_4, *p*-C_6H_2-2,6-Me_2, *p*-C_6Me_4, and *p*-C_6H_4-2,6-*t*Bu_2.[5] On the basis of IR spectroscopic data (ν(N≡C)) for free and coordinated ligands, these materials were described as large polymers. Except for XPS data, no further analysis was provided. Our group has also recently reported several series of Pd−Pd and Pt−Pt bond-containing coordination/organometallic polymers using di- $(Pd_2(dmb)_2^{2+}$ and (diphos)Pd−Pd(diphos)$^{2+}$, diphos = $Ph_2P(CH_2)_nPPh_2$, n = 2−6) and tetranuclear building blocks ($M_4(dmb)_4^{2+}$, Chart 1). These materials did not exhibit π-delocalization between the M−M fragments.[6] The aryl diisocyanide-containing polymers show promise for new materials with respect to "electronic communication" along the polymer backbone. A detailed investigation now appears to be required to address the structural, physical, electronic, and photophysical properties of these materials in solution and in the solid state.

We now wish to report the syntheses of conjugated rigid rod and nonconjugated flexible polymers and corresponding

* To whom correspondence should be addressed. E-mail: Pierre.Harvey@USherbrooke.ca.
(1) Université de Sherbrooke. (b) University of New Brunswick.

(2) Manners, I. *Science* **2001**, *294*, 1664. (b) Manners, I. *Synthetic Metal-Containing Polymers*; Wiley-VCH: Weinheim, Germany, 2004. (c) Newkome, G. R.; He, E.; Moorefield, C. N. *Chem. Rev.* **1999**, *99*, 1689−1746. (d) Astruc, D.; Chardac, F. *Chem. Rev.* **2001**, *101*, 2991. (e) Abd-El-Aziz, A. S., Ed. *Macromol. Symp.* **2003**, *196*, 1. (e) Abd-El-Aziz, A. S., Harvey, P. D., Eds. *Macromol. Symp*. **2004**, *209*, 1. (f) Kingsborough, R. P.; Swager, T. M. *Prog. Inorg. Chem.* **1999**, *48*, 123. (g) Wolf, M. O. *Adv. Mater.* **2001**, *13*, 545. (h) Archer, R. D. *Inorganic and Organometallic Polymers*; John Wiley & Sons Inc.: New York, 2001. (i) Abd-El-Aziz, A. S., Carraher, C. E., Jr., Pittman, C. U., Jr., Sheats, J. E., Zeldin, M., Eds. *Macromolecule Containing Metal and Metal-like Elements*; Wiley-Interscience: New York, 2005; Vol. 5.

10.1021/ic0509480 CCC: $33.50
Published on Web 03/02/2006

Chart 1

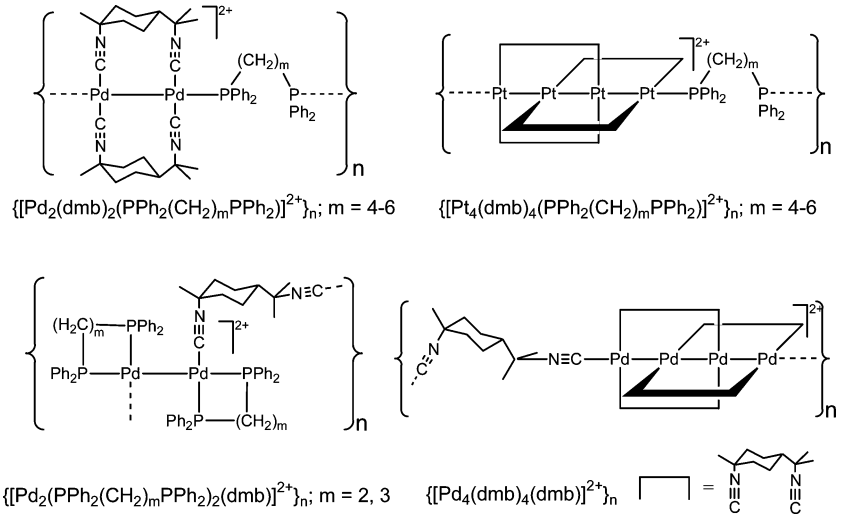

model compounds bearing the d^9-d^9 $M_2(dppm)_2^{2+}$ fragments (M = Pd, Pt, Chart 2, the counterion is BF_4^- in all cases). These d^9-d^9 $M_2(dppm)_2^{2+}$ were selected because the M−M-bonded units are easily characterized from a spectroscopic stand point (NMR, IR, UV−vis). Any perturbation, such as band shifts would easily be interpretable. In addition, the presence of π-delocalization between the $M_2(dppm)_2$ fragments is better addressed using the comparison between aryl- and alkyl-diisocyanide assembling ligands. These new materials are thoroughly characterized using techniques such as TGA, DSC, XRD, and light scattering measurements. The effects of conjugation, chain flexibility, and of the metal are examined, along with their electronic and photophysical properties, in solution and in the solid state at 298 and 77 K. During the course of this investigation, the X-ray structures of **M1**, **M3**, and **M4** have been determined.

Experimental Section

Materials. $Pd_2(dppm)_2Cl_2$,[7] $Pt_2(dppm)_2Cl_2$,[7] $[Pd_2(dppm)_2(NCCH_3)_2](PF_6)_2$,[8] $[Pt_2(dppm)_2(NCCH_3)_2](PF_6)_2$,[8] $[Pt_2(dppm)_2(2,5\text{-}CNC_6Me_2H_3)_2](BF_4)_2$,[5] 1-isocyano-2,5-dimethylbenzene,[9] 4-diisocyano-2,3,5,6-tetramethylbenzene,[9] 1,8-diisocyano-p-menthane,[9] 1-isocyano-2,6-dimethylbenzene,[9] and 1-isocyano-4-isopropylbenzene[9] were prepared according to standard procedures. The following materials were purchased from commercial suppliers: dppm (Aldrich), *t*-BuNC (Aldrich), $PdCl_2$ (Pressure Chemical), K_2PtCl_4 (Strem), acetone (Fisher), acetonitrile, petroleum ether, dichloromethane (ACP), ethanol (Les Alcools de Commerce Inc.), PrCN (Aldrich), dinitrogen, and argon (Praxair). All solvents were dried and distilled prior to use. For acetonitrile and PrCN, the emission spectra for these solvents were verified prior to use. No or weak emissions were detected and were easily subtracted from the emissions of the samples when necessary. Unless otherwise stated, all materials were handled under Ar or N_2 using standard Schlenk techniques, high-vacuum manifolds, and an inert-atmosphere glovebox. The elemental analyses were performed at the Université de Montréal, and the presence of water was confirmed by ^1H NMR and IR spectroscopy in all cases.

(3) Caliendo, C.; Fratoddi, I.; Russo, M. V.; Lo Sterzo, C. *J. Appl. Phys.* **2003**, *93* (12), 10071. (b) Onitsuka, K.; Shimizu, A.; Takahashi, S. *Chem. Commun*. **2003**, 280. (c) Iucci, G.; Polzonetti, G.; Altamura, P.; Paelucci, G.; Goldoni, A.; Russo, M. V. *J. Vac. Sci. Technol. A* **2000**, *18* (1), 248. (d) Wong, W.-Y.; Chan, S.-M.; Choi, K.-H.; Cheah, K.-W.; Chan, W.-K. *Macromol. Rapid Commun.* **2000**, *21*, 453. (e) Matsumoto, F.; Matsumi, N.; Chupio, Y. *Polym. Bull.* **2001**, *46*, 257. (f) Onitsuka, K.; Iuchi, A.; Fujimoto, M.; Takahashi, S. *Chem. Commun.* **2001**, *741*. (g) Iucci, G.; Infante, G.; Polzonetti, G. *Polymer* **2002**, *43*, 655. (h) Wong, W.-Y.; Choi, K.-H.; Lu, G.-L.; Shi, J.-X. *Macromol. Rapid Commun.* **2001**, *22*, 461. (i) Köhler, A.; Wittman, H. F.; Friend, R. H.; Khan, M. S.; Lewis, J. *Synth. Met.* **1996**, *77*, 147. (j) Belluco, U.; Bertani, R.; Michelin, R. A.; Mozzon, M. *J. Organomet. Chem.* **2000**, *600*, 37. (k) Fratoddi, I.; Altamura, P.; Sterzo, C. L.; Furlani, A.; Galassi, E.; D'Amico, A.; Russo, M. V. *Polym. Adv. Technol*. **2002**, *13*, 269. (l) Caliendo, C.; Fratoddi, I.; Russo, M. V.; Sterzo, C. L. *J. Appl. Phys.* **2003**, *93*, 10071. (m) D'Amato, R.; Fratoddi, I.; Coppotto, A.; Altamura, P.; Delfini, M.; Bianchetti, C.; Bolasco, A.; Polzonetti, G.; Russo, M. V. *Organometallics* **2004**, 23, 2860. (n) Khan, S. Al-Mandhary, M. R. A.; Al-Suti, M. K.; Al-Battashi, F. R.; Al-Saadi, S.; Ahrens, B.; Bjernemose, J. K.; Mahon, M. F.; Raitby, P. R.; Younous, M.; Chawdhury, N.; Kohler, A.; Marseglia, E. A.; Tedesco, E.; Feeder, N.; Teat, S. *J. Dalton Trans.* **2004**, 2377. (o) Wong, W.-Y.; Wong, C.-K.; Lu, G.-L.; Lee, A. W.-M.; Cheah, K.-W.; Shi, J.-X. *Macromolecules* **2003**, *36*, 983. (p) Wilson, J. S.; Chawdhury, N.; Köhler, A; Friend, R. H.; Al-Mandhary, M. R. A.; Khan, M. S.; Younus, M.; Raithby, P. R. *J. Am. Chem. Soc.* **2001**, *123*, 9412. (q) Wong, W.-Y.; Liu, Li; Poon, S.-Y.; Choi, K.-H.; Cheah, K.-W.; Shi, J.-X. *Macromolecules* **2004**, *37*, 4496. (r) Wong, W.-Y.; Poon, S.-Y.; Lee, A. W.-M.; Shia, J.-X.; Cheah, K.-W. *Chem. Commun.* **2004**, 2420. (s) Tanase, T.; Goto, E.; Begum, R. A.; Hamaguchi, M.; Zhan, S.; Iida, M.; Sakai, K. *Organometallics* **2004**, *23*, 5975. (t) Harvey, P. D. *Macromolecule Containing Metal and Metal-like Elements*; Abd-El-Aziz, A. S., Carraher, C. E., Jr., Pittman, C. U., Jr., Sheats, J. E., Zeldin, M., Eds.; Wiley-Interscience: New York, 2005; Vol. 5, Chapter 4, p 83.

(4) Phang, L.-T.; Gan, K.-S.; Lee, H.-L.; Hor, T. S. A. *J. Chem. Soc., Dalton Trans.* **1993**, 2697. (b) Kerby, M. C.; Eichorn, B. W.; Creighton, J. A.; Vollhardt, K. P. C. *Inorg. Chem.* **1990**, *29*, 1319. (c) Kerby, M. C.; Eichorn, B. W.; Creighton, J. A.; Vollhardt, K. P. C. *Organomet. Polym.* **1990**, *1*, 288. (d) Deeming, A. J.; Nuel, D.; Randle, N. P.; Whittaker, C. *Polyhedron* **1989**, *8*, 1537. (e) Sherlock, S. J.; Cowie, M.; Singleton, E.; Steyn, M. M. de V. *Organometallics* **1988**, *7*, 1663.

(5) Irwin, M. J.; Jia, G.; Viital, J. J.; Puddephatt, R. *Organometallics* **1996**, *15*, 5321.

(6) Sicard, S.; Bérubé, J.-F.; Samar, D.; Massaoudi, A.; Lebrun, F.; Fortin, J.-F.; Fortin, D.; Harvey, P. D. *Inorg. Chem.* **2004**, *43*, 5321. (b) Fournier, É.; Sicard, S.; Decken, A.; Harvey, P. D. *Inorg. Chem.* **2004**, *43*, 1491. (d) Zhang, T.; Drouin, M.; Harvey, P. D. *Inorg. Chem.* **1999**, *38*, 1305. (e) Zhang, T.; Drouin, M.; Harvey, P. D. *Inorg. Chem.* **1999**, *38*, 957.

(7) Balch, A. L.; Benner, L. S. *Inorg. Synth.* **1982**, *21*, 47. (b) Grossel, M. C. *J. Organomet. Chem.* **1986**, *304*, 391. (c) Brittingham, K. A.; Schreider, S.; Gallaher, T. N. *J. Chem. Educ.* **1995**, *72*, 941.

(8) Benner, L. S.; Balch, A. L. *J. Am. Chem. Soc.* **1978**, *100*, 6099. (b) Rashidi, M.; Vittal, J. J.; Puddephatt, R. J. *J. Chem. Soc., Dalton Trans.* **1994**, 1283.

(9) Weber, W. P.; Gokel, G. W. *Tetrahedron Lett*. **1972**, *17*, 1637.

Chart 2

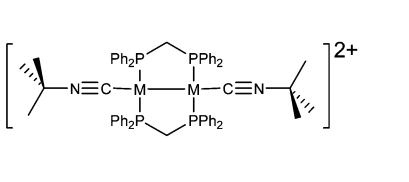

M = Pd (**M1**), Pt(**M3**)

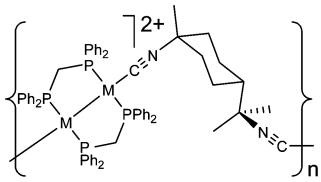

M = Pd (**P1**), Pt(**P3**)

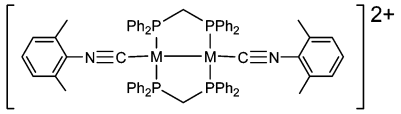

M = Pd (**M2**)

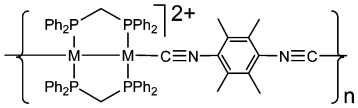

M = Pd (**P2**), Pt(**P4**)

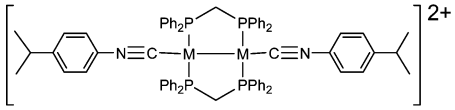

M = Pt(**M4**)

[Pd$_2$(dppm)$_2$(CN-*t*-Bu)$_2$](BF$_4$)$_2$ (M1). Pd$_2$(dppm)$_2$Cl$_2$ (0.205 g, 0.195 mmol) and NaBF$_4$ (0.471 g, 4.29 mmol) were placed under nitrogen in a Schlenk flask. Water (30 mL), followed by dichloromethane (30 mL), was added to the flask. A solution (3.59 mL) of *tert*-butyl isocyanide (0.390 mmol) in acetonitrile was added dropwise to the solution. The reaction was stirred at 298 K overnight. The organic layer was washed with water (3 × 20 mL), dried with MgSO$_4$, filtered, and concentrated to 15 mL under vacuum. Diethyl ether (250 mL) was added to the solution; an orange precipitate appeared and was filtered. The solid was dried under vacuum for 24 h (0.183 g.) Yield: 82%.^{1}H NMR (CD$_2$Cl$_2$): δ 7.53−7.30 (m, 40H, Ph), 4.65 (q, 4H, PCH$_2$P, $^2J_{H-P}$= 4.9 Hz, $^4J_{H-P}$= 4.7 Hz), 0.73 (s, 18H, C(CH$_3$)$_3$). ^{31}P NMR (CD$_2$Cl$_2$): δ −1.2. IR (KBr): ν 2187 cm^{-1} (C≡N). Anal. Calcd for Pd$_2$C$_{60}$H$_{62}$B$_2$F$_8$N$_2$P$_4$·0.9 H$_2$O (1321.492): C, 53.87; H, 4.81; N, 2.09. Found: C, 53.85; H, 4.81; N, 2.19. MALDI-TOF (mass *m*/*z*): 1266.7 (**M1** − C$_4$H$_9$), 1094.7 (**M1** − 2(C$_4$H$_9$) − BF$_4$ − CN), 979.8 (**M1** − 2(C$_4$H$_9$) − 2(BF$_4$) − 2(CN)).

{**[Pd$_2$(dppm)$_2$(dmb)](BF$_4$)$_2$**}$_n$ **(P1). P1** was synthesized from Pd$_2$(dppm)$_2$Cl$_2$ (0.242 g, 0.230 mmol), NaBF$_4$ (0.505 g, 4.60 mmol), and the ligand dmb (0.0438 g, 0.230 mmol) according to the procedure described above. The dmb was added dropwise to the solution with 2−3 mL of dichloromethane. An orange precipitate appeared and was removed by filtration: it was washed with water (3 × 10 mL), filtered again, dissolved in CH$_3$CN, and precipitated with 450 mL of diethyl ether (0.240 g). Yield: 77%. ^{1}H NMR (CD$_3$CN): δ 7.65−7.15 (m, 40H, Ph), 4.65 (m, 4H, PCH$_2$P), 0.40 between 0.88 and 0.07 (m, 18H, dmb). ^{31}P NMR (CD$_3$CN): δ 0.7. IR (KBr): ν 2178 cm^{-1} (C≡N). Anal. Calcd for Pd$_2$C$_{62}$H$_{62}$B$_2$F$_8$N$_2$P$_4$·0.3H$_2$O (1345.513): C, 55.12; H, 4.67; N, 2.07. Found: C, 55.15; H, 4.50; N, 2.33. MALDI-TOF (mass *m*/*z*): 1258.7 (**P1** − BF$_4$), 1169.7 (**P1** − 2(BF$_4$)), 980.9 (**P1** − 2(BF$_4$) − dmb).

[Pd$_2$(dppm)$_2$(CN-C$_8$H$_9$)$_2$](BF$_4$)$_2$ (M2). M2 was synthesized from Pd$_2$(dppm)$_2$Cl$_2$ (0.302 g, 0.287 mmol), NaBF$_4$ (0.630 g, 5.73 mmol), and the ligand 1-isocyano-2,6-dimethylbenzene (0.0833 g, 0.573 mmol) according to the procedure described for **M1**. 1-Isocyano-2,6-dimethylbenzene was added dropwise to the solution with 2−3 mL of dichloromethane. Yellow product (0.371 g). Yield: 89%.^{1}H NMR (CD$_2$Cl$_2$): δ 7.50−7.15 (m, 40H, Ph), 7.15−7.00 (t, 2H, CH$_{para}$-Xyl, $^3J_{H-H}$= 7.5 Hz), 6.95−6.80 (d, 4H, CH$_{meta}$-Xyl, $^3J_{H-H}$= 7.6 Hz), 4.83 (s, 4H, PCH$_2$P), 1.71 (s, 12H, CH$_3$). ^{31}P NMR (CD$_2$Cl$_2$): δ −1.5 ppm. IR (KBr): ν 2168 cm^{-1} (C≡N). Anal. Calcd for Pd$_2$C$_{68}$H$_{66}$B$_2$F$_8$N$_2$P$_4$·1.8 H$_2$O (1421.61): C, 56.17; H, 4.82; N, 1.93. Found: C, 56.20; H, 4.63; N, 2.29.

{**[Pd$_2$(dppm)$_2$(CNC$_6$(CH$_3$)$_4$NC)](BF$_4$)$_2$**}$_n$ **(P2). P2** was synthesized from Pd$_2$(dppm)$_2$Cl$_2$ (0.395 g, 0.375 mmol), NaBF$_4$ (0.906 g, 8.26 mmol), and the ligand 1,4-diisocyano-2,3,5,6-tetramethylbenzene (0.692 g, 0.375 mmol) according to the procedure described for **P1**. Orange product (0.453 g). Yield: 90%. ^{1}H NMR (CD$_3$CN): δ 7.44−7.21 (m, 40H, Ph), 4.90 (s, 4H, PCH$_2$P), 1.42 (s, 12H, CH$_3$). ^{31}P NMR (CD$_3$CN): δ 1.4. IR (KBr): ν 2167 cm^{-1} (C≡N). Anal. Calcd for Pd$_2$C$_{62}$H$_{56}$B$_2$F$_8$N$_2$P$_4$·1.1 H$_2$O (1339.46): C, 54.78; H, 4.32; N, 2.06. Found: C, 54.75; H, 4.48; N, 2.09. MALDI-TOF (mass *m*/*z*): 1094.7 (**P2** − BF$_4$ − C$_{10}$H$_{12}$CN), 980.9 (**P2** − 2(BF$_4$) − CNC$_{10}$H$_{12}$CN).

[Pt$_2$(dppm)$_2$(CN-*t*-Bu)$_2$](BF$_4$)$_2$ (M3). M3 was synthesized from Pt$_2$(dppm)$_2$Cl$_2$ (0.270 g, 0.220 mmol), NaBF$_4$ (0.482 g, 4.39 mmol) according to the procedure described for **M1**. A solution of *t*-BuNC in acetonitrile (4.04 mL, 0.439 mmol) was added dropwise to the solution. Beige-yellow product (0.264 g). Yield: 80%. ^{1}H NMR (CD$_3$CN): δ 7.57−7.50 (m, 8H, Ph), 7.39−7.30 (m, 32H, Ph), 5.15 (t of pseudo quint., 4H, PCH$_2$P, $^2J_{H-P}$= 4.9 Hz, $^4J_{H-P}$= 4.7 Hz,$^3J_{H-Pt}$= 29.4 Hz), 0.60 (s, 18H, C(CH$_3$)$_3$). ^{31}P NMR (CD$_3$CN): δ −1.5 (s + d (^{195}Pt, 33.8%), $^1J_{Pt-P}$= 2546 Hz). IR (KBr): ν 2187 cm^{-1} (C≡N). Raman: ν 2192 (C≡N), 177 (PtP), 137 (PtPt, shoulder) cm^{-1}. Anal. Calcd for Pt$_2$C$_{60}$H$_{62}$B$_2$F$_8$N$_2$P$_4$·0.7H$_2$O (1498.808): C, 47.68; H, 4.23; N, 1.85. Found: C, 47.66; H, 4.22; N, 2.17. MALDI-TOF (mass *m*/*z*): 1410.8 (**M3** − BF$_4$), 1239.9 (**M3** − 2BF$_4$ − CN-*t*-Bu).

{**[Pt$_2$(dppm)$_2$(dmb)](BF$_4$)$_2$**}$_n$ **(P3). P3** was synthesized from Pt$_2$(dppm)$_2$Cl$_2$ (0.202 g, 0.164 mmol), NaBF$_4$ (0.360 g, 3.22 mmol), and dmb (0.0312 g, 0.164 mmol) according to the procedure described for **P1**. Orange product (0.184 g). Yield: 73%. ^{1}H NMR (CD$_3$CN): δ 7.65−7.05 (m, 40H, Ph), 5.08 (m, 4H, PCH$_2$P), 0.0 between 0.65 and −0.65 (m, 18H, dmb). ^{31}P NMR (CD$_3$CN): δ 1.45 (m + d (^{195}Pt, 33.8%) of m, $^1J_{Pt-P}$= 2580 Hz). IR (KBr): ν

2181 cm^{-1} (C≡N). Raman: ν 2183 (C≡N), 177 (PtP), 137 (PtPt, shoulder) cm^{-1}. Anal. Calcd for $Pt_2C_{62}H_{62}B_2F_8N_2P_4 \cdot 3.6\ H_2O$ (1522.829): C, 46.90; H, 4.39; N, 1.76. Found: C, 46.90; H, 4.20; N, 1.76. MALDI-TOF (mass *m*/*z*): 1347.9 (**P3** − $2BF_4$), 1157.0 (**P3** − $2BF_4$ − dmb).

$[Pt_2(dppm)_2(CNC_6H_4$-*i*-Pr$)_2](BF_4)_2$ (M4). M4 was synthesized from $Pt_2(dppm)_2Cl_2$ (0.728 g, 0.592 mmol), $NaBF_4$ (1.30 g, 11.8 mmol), and 1-isocyano-4-isopropylbenzene (0.171 g, 1.18 mmol) according to the procedure described for **M1**. 1-Isocyano-4-isopropylbenzene was added dropwise to the solution with 2−3 mL of dichloromethane. Orange product (0.614 g). Yield: 64%. ^{1}H NMR (CD_3CN): δ 7.54−7.30 (m, 40H, Ph), 6.95 (d, 4H, (CH_{meta})-CNC_6H_4, J_{H-H}= 8.4 Hz), 6.00 (d, 4H, (CH_{ortho})-CNC_6H_4, J_{H-H}= 8.2 Hz), 5.27 (t of pseudo quint., 4H, PCH_2P, $^2J_{H-P}$= 4.8 Hz, $^4J_{H-P}$= 4.7 Hz, $^3J_{H-Pt}$= 29.0 Hz), 2.77 (sept., 2H, C*H*$(CH_3)_2$, J_{H-H}= 6.9 Hz), 1.10 (d, 12H, CH(C*H*$_3)_2$, J_{H-H}= 6.9 Hz). ^{31}P NMR (CD_3CN): δ −1.5 (s + d (^{195}Pt; 33.8%), $^1J_{Pt-P}$= 2471 Hz). IR (KBr): ν 2163 cm^{-1} (C≡N). Raman: ν 2172 (C≡N), 177 (PtP), 133 (PtPt, shoulder) cm^{-1}. Anal. Calcd for $Pt_2C_{70}H_{66}B_2F_8N_2P_4 \cdot 1.3H_2O$ (1622.947): C, 51.07; H, 4.20; N, 1.70. Found: C, 51.06; H, 4.10; N, 1.67. MALDI-TOF (mass *m*/*z*): 1534.8 (**M4** − BF_4), 1301.9 (**M4** − $2BF_4$ − CN − C_9H_{11}).

$\{[Pt_2(dppm)_2(CN$-$C_{10}H_{12}$-NC)$](BF_4)_2\}_n$ (P4). P4 was synthesized from $Pt_2(dppm)_2Cl_2$ (0.531 g, 0.432 mmol), $NaBF_4$ (0.949 g, 8.64 mmol), and 1,4-diisocyano-2,3,5,6-tetramethylbenzene (0.0796 g, 0.432 mmol) according to the procedure described for **P1**. Dark orange product (0.504 g). Yield: 77%. ^{1}HNMR (CD_3CN): δ 7.55−7.05 (m, 40H, Ph), 5.31 (m, 4H, PCH_2P), 1.33 (s, 12H, CH_3). ^{31}P NMR (CD_3CN): δ 1.6 (s + d (^{195}Pt, 33.8%), $^1J_{Pt-P}$= 2508 Hz). IR: ν 2148 cm^{-1} (C≡N). Raman: ν 2165 (C≡N), 177 (PtP), 134 (PtPt, shoulder) cm^{-1}. Anal. Calcd for $Pt_2C_{62}H_{56}B_2F_8N_2P_4 \cdot 2.6H_2O$ (1516.782): C, 47.63; H, 3.95; N, 1.79. Found: C, 47.60; H, 3.73; N, 1.92. MALDI-TOF (mass *m*/*z*): 1340.9 (**P4** − $2BF_4$), 1157.0 (**P4** − $2BF_4$ − CN − $C_{10}H_{12}$ −NC).

Apparatus. All NMR spectra were acquired with a Bruker AC-300 spectrometer (^{1}H 300.15 MHz, ^{13}C 75.48 MHz, ^{31}P 121.50 MHz) using the solvent as the chemical shift standard, except in ^{31}P NMR, where the chemical shifts are relative to D_3PO_4 85% in D_2O. All chemical shifts (δ) are given in ppm. The IR spectra were acquired on a Bomem FT-IR MB series spectrometer equipped with a baseline-diffused reflectance. FT-Raman spectra were acquired on a Bruker RFS 100/S spectrometer. The UV−vis spectra were measured on a HP 8452A diode array spectrophotometer. The emission lifetimes were measured with a nanosecond N_2 laser system from PTI model GL-3300 pumping a dye laser model GL-302. The pulse width was 2 ns, and the lower limit for the measurements was approximately 150 ps after deconvolution. The excitation wavelength was 325−385 nm, as close as possible to the d$\sigma \rightarrow$dσ^* absorption. The continuous-wave emission spectra were also measured on a SPEX Fluorolog II. The glass transition temperature (T_g) was determined using a Perkin-Elmer 5A DSC7 equipped with a thermal controller 5B TAC 7/DS. Calibration standards were water and indium. The accuracy was ±0.1 °C and ±0.1% for ΔCp. The sample weights ranged from 5 to 10 mg, and the scan rate was adjusted to 10°/min. XRD data were acquired on a Rigaku/USA Inc X-ray powder diffractometer with a copper lamp operating under a 30 mA current and a 40 KV tension. TGA were acquired on a Perkin-Elmer TGA 7 between 50 and 950 °C at 3 °C/ min under a nitrogen atmosphere. The pictures of the X-ray powder diffraction were obtained at 293 K on an Enraf Nonius CAD-4 automatic diffractometer and on a Hitachi S4700 spectrometer operating at a voltage of 15kV, with a working distance (WD) of 12 mm, a magnification of 500×, and an acquisition time of 300 s. The EI mass spectra were obtained on a VG Micromass Zab-1F spectrometer. The data analyses were performed using a homemade program written in GW BASIC, computing all mathematically possible solutions for each fragment mass. Only the chemically meaningful solutions were retained using a window of ±2 g.

Spin−Lattice Relaxation Times (T_1) and Nuclear Overhauser Enhancement (NOE). The T_1's were measured by inversion recovery pulse technique. The measurements were performed on a Bruker AC-F 300 NMR spectrometer operating at 121.50 MHz for ^{31}P. The temperature was 293 K, and the sampling was done over a 20 000 Hz sweep width using 8192 data points to describe the FID. The solutions were saturated in all cases to improve the signal-to-noise ratio. The uncertainties are ±0.05 s based on multiple measurements (at least 3). The NOE constants were measured using the inverse-gated method. On the basis of the reproducibility of the measurements, the accuracy of the method is estimated to be ±10%. The internal standard (PBr_5) was inside a sealed capillary tube to avoid contact with the samples.

Light Scattering. The d*n*/d*c* (*n* = refractive index, *c* = concentration) for **P1**−**P4**, necessary for the M_w measurements, were obtained using an OPTILAB DSP interferometric refractometer. The polymer concentrations were 0.2, 0.4, 0.6, and 0.8 mg/mL in HPLC grade acetonitrile, and the solutions were filtered using 0.02 μm Millipore filters for **P1** and **P3** and 0.2 μm filters for **P2** and **P4** prior to the measurements. The M_w were measured using a Dawn Ose instrument from Wyatt Technology. The apparatus was stabilized 12 h prior to each measurement. The light source was a GaAs solid-state laser irradiating at 690 nm where no absorption was possible.

Intrinsic Viscosity. The intrinsic viscosity measurements were performed using a A508 CANNON viscosimeter. This instrument was verified against the universal standard polymethyl methacrylate from Aldrich (M_n = 12 000, 15 000, 120 000, and 320 000). The measurements were reproduced five times for greater accuracy. The results were compared to the known oligomer $\{[Ag(dmb)_2]BF_4\}_n$ (M_n = 4000).[10]

Computer Modeling. The calculations of the space filling models were performed using the commercially available PC model from Serena Software (version 7.0), which uses the MMX empirical model. No constraint on bond distances and angles was applied to ensure that deviations from normal geometry are depicted. The R−N≡C groups were replaced by R−C≡C$^-$ because the PC model does not model C≡N$^+$ fragments properly, resulting in strongly bent structures. Instead −C≡C− is used, securing a more linear and realistic frame for the ligand. This method is qualitative.

Theoretical Computations. The density functional theory (DFT) calculations were performed using the commercially available Gaussian 98 software and a Pentium 4 computer (1.6 G).[11] The computations for geometry optimization and frontier molecular

(10) Turcotte, M.; Harvey, P. D. *Inorg. Chem.* **2002**, *41*, 1739−1746.
(11) Frisch, M. J.; Trucks, G. W.; Schlegel, H. B.; Scuseria, G. E.; Robb, M. A.; Cheeseman, J. R.; Zakrzewski, V. G.; Montgomery, J. A., Jr.; Stratmann, R. E.; Burant, J. C.; Dapprich, S.; Millam, J. M.; Daniels, A. D.; Kudin, K. N.; Strain, M. C.; Farkas, O.; Tomasi, J.; Barone, V.; Cossi, M.; Cammi, R.; Mennucci, B.; Pomelli, C.; Adamo, C.; Clifford, S.; Ochterski, J.; Petersson, G. A.; Ayala, P. Y.; Cui, Q.; Morokuma, K.; Malick, D. K.; Rabuck, A. D.; Raghavachari, K.; Foresman, J. B.; Cioslowski, J.; Ortiz, J. V.; Stefanov, B. B.; Liu, G.; Liashenko, A.; Piskorz, P.; Komaromi, I.; Gomperts, R.; Martin, R. L.; Fox, D. J.; Keith, T.; Al-Laham, M. A.; Peng, C. Y.; Nanayakkara, A.; Gonzalez, C.; Challacombe, M.; Gill, P. M. W.; Johnson, B. G.; Chen, W.; Wong, M. W.; Andres, J. L.; Head-Gordon, M.; Replogle, E. S.; Pople, J. A. *Gaussian 98*, revision A.6; Gaussian, Inc.: Pittsburgh, PA, 1998.

Scheme 1

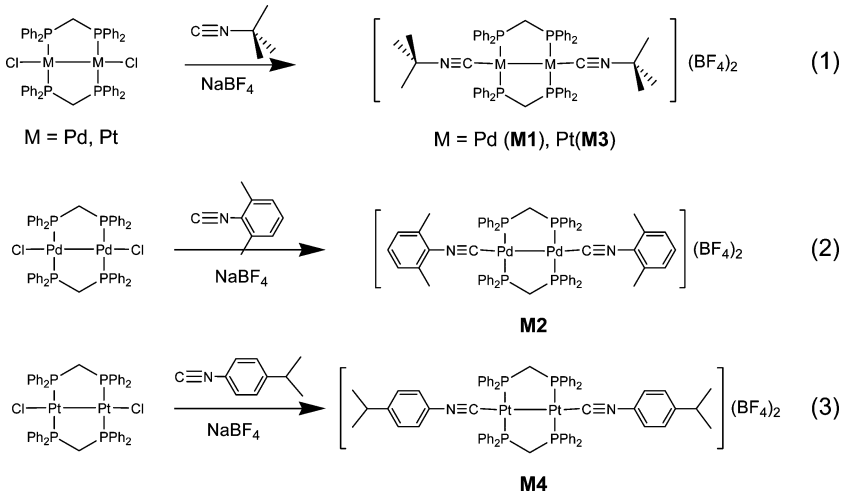

orbitals were performed at the RB3LYP level (Becke's three parameter hybrid functional[12] using the LYP (Lee−Yang−Parr) correlation functional).[13] The basis set for the polarization and diffuse function was the 3-21G* set.[14] To save computation time, dppm was replaced with the $PH_2CH_2PH_2$ bridging ligand.

Conductivity Measurements. The conductivity measurements were performed on a homemade four-point probe apparatus designed according to S. M. Sze.[15] The samples were pressed pellets with a surface area of 1.13 cm^2. The potentials were measured with a standard Keithley 177 μV DMM voltmeter, and the applied current was generated with a TRYGON model HH32-1.5 Systron-Donner Corp. source operating at 1.5 A between 0 and 32 V. The precision was ±1%.

X-ray Structures. The general procedure for data collection and analyses are available in the Supporting Information.[16−21]

$[Pd_2(dppm)_2(CN\text{-}t\text{-}Bu)_2](BF_4)_2$ (M1). The crystal was grown by vapor diffusion of ethyl acetate/acetonitrile at room temperature. The reflections were acquired at 198(2) K. Two standard reflections were measured every 100 reflections, and no significant intensity decay was observed during data collection. The non-hydrogen atoms were refined anisotropically. The hydrogen atoms were placed at idealized calculated geometric positions and refined isotropically using a riding model. Disorder was found on the BF_4 anion sites, and the bond distances were fixed to the ideal values; equal thermal values (EADP) were used for refinement.

$[Pt_2(dppm)_2(CNC_6H_4\text{-}i\text{-}Pr)_2](BF_4)_2$ (M4). The crystal was grown by vapor diffusion of ethylmethylketone/*tert*-butylmethyl ether at room temperature. Single crystals were coated with Paratone-N oil, mounted using a glass fiber and frozen in the cold nitrogen stream of the goniometer. All non-hydrogen atoms were refined anisotropically. Hydrogen atoms were included in calculated positions and refined using a riding model.

$[Pt_2(dppm)_2(CN\text{-}t\text{-}Bu)_2](BF_4)_2$ (M3). The crystal was grown by vapor diffusion using ethanol/hexane at room temperature. One single crystal was mounted using a glass fiber on the goniometer. Data were collected at 293(2) K. Two standard reflections were measured every 100 reflections, no significant intensity decay was observed during data collection. The non-hydrogen atoms were refined anisotropically. The hydrogen atoms were placed at idealized calculated geometric positions and refined isotropically using a riding model. The absolute structure was refined using TWIN[22] to deal with the anomalous dispersion effects. The final refined BASF factor found was 0.24. Disorder was found on the BF_4 anion sites; the bond distances were fixed to the ideal values, and equal thermal values (EADP) were used for refinement. Idealized phenyl rings and similar thermal and bond restraints (SIMU, DELU) were also used to refine the phenyl groups. The N≡C and C−C bonds (C−CH_3) were also fixed to ideal values prior to refinement.

Results and Discussion

I. Syntheses and Characterization of the Model Compounds. The compounds were synthesized as shown in Scheme 1 via a substitution reaction of the chloride by the isocyanide ligand accompanied by the dissolution of NaCl in the aqueous phase. The model compounds exhibit mass spectra in which peaks for the complete salt formula were never observed, indicating the relative fragility of the compounds. No signal indicating the presence of Cl-containing fragments (easily recognizable by the isotopic distribution) was observed, suggesting a quantitative substitution. Concurrently, electron diffraction scattering (EDS) measurements did not exhibit peaks associated with the presence of Cl.

The vibrational activity of the ν(C≡N) modes (**M3** IR 2187, Raman 2192; **M4** IR 2163, Raman 2172 cm^{-1}) where the inequality between the IR and Raman spectroscopic data is indicative of a center of inversion within the $Pt_2(dppm)_2^{2+}$ fragment. The presence of the M−M bonds in the model

(12) Becke, A. D. *J. Chem. Phys.* **1993**, *98*, 5648.
(13) Lee, C.; Yang, W.; Parr, R. G. *Phys. Rev.* **1988**, *B 37*, 785. (b) Miehlich, A. D.; Savin, A.; Stoll, H.; Preuss, H. *Chem. Phys. Lett.* **1989**, *157*, 200.
(14) Dobbs, K. D.; Hehre W. J. *J. Comput. Chem.* **1986**, *7*, 359; (b) *J. Comput. Chem.* **1987**, *8*, 861; (c) *J. Comput. Chem.* **1987**, *8*, 880.
(15) Sze, S. M. *Physics of Semiconductors*, 2nd ed; John Wiley: Toronto, Canada, 1981; pp 30−32.
(16) Flack, H. D.; Blanc, E.; Schwarzenbach, D. *J. Appl. Crystallogr.* **1992**, *25*, 455−459.
(17) Gabe, E. J.; Le Page, Y.; Charland, J.-P.; Lee, F. L.; White, P. S. *J. Appl. Crystallogr.* **1989**, *22*, 384−387.
(18) Sheldrick, G. M. *SHELXS-97*, release 97-2; University of Göttingen: Göttingen, Germany, 1997.
(19) *SAINT*, version 6.02; Bruker AXS, Inc.: Madison, WI, 1997−1999.
(20) Sheldrick, G. *SADABS*; Bruker AXS, Inc.: Madison, WI, 1999.
(21) *SHELXTL*, version 6.14; Bruker AXS, Inc.: Madison, WI, 2000−2003.
(22) *GEMINI*, version 1.0; Bruker AXS, Inc.: Madison, WI, 1999.

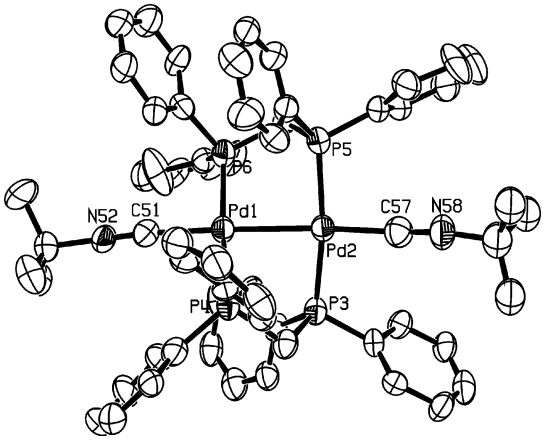

Figure 1. ORTEP representation of **M1**. The ellipsoids are shown at 30%, and the hydrogen atoms and counteranions are not shown for clarity. Selected bond lengths (Å): Pd(1)−Pd(2) = 2.6186(12), P(6)−Pd(1) = 2.312(4), P(4)−Pd(1) = 2.311(4), P(5)−Pd(2) = 2.296(4), P(3)−Pd(2) = 2.272(4), C(57)−Pd(2) = 1.989(15), C(51)−Pd(1) = 2.011(13), C(51)−N(52) = 1.117(15), C(51)−N(52) = 1.117(15). Selected angles (deg): N(52)−C(51)−Pd(1) = 175.0(12), N(58)−C(57)−Pd(2) = 165.5(14), C(51)−Pd(1)−Pd(2) = 177.0(4), C(57)−Pd(2)−Pd(1) = 170.8(5), P(4)−Pd(1)−P(6) = 173.55(13), P(3)−Pd(2)−P(5) = 169.16(13).

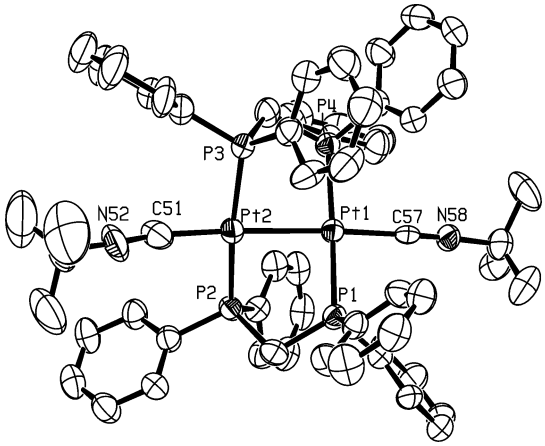

Figure 2. ORTEP representation of **M3**. The ellipsoids are shown at 30%, and the hydrogen atoms and counteranions are not shown for clarity. Selected bond lengths (Å): Pt(1)−Pt(2) = 2.6355(8), P(4)−Pt(1) = 2.306(4), P(3)−Pt(2) = 2.276(4), P(2)−Pt(2) = 2.276(4), P(1)−Pt(1) = 2.298(4), C(57)−Pt(1) = 2.011(13), C(51)−Pt(2) = 1.946(17), C(51)−N(52) = 1.185(16), C(57)−N(58) = 1.131(14). Selected angles (deg): N(52)−C(51)−Pt(2) = 163(2), N(58)−C(57)−Pt(1) = 177.9(16), N(58)−C(57)−Pt(1) = 177.9(16), C(57)−Pt(1)−Pt(2) = 177.2(4), P(1)−Pt(1)−P(4) = 174.46(14), P(3)−Pt(2)−P(2) = 170.97(15).

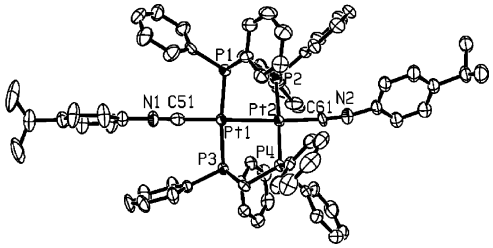

Figure 3. ORTEP representation of **M4**. The ellipsoids are shown at 30%, and the hydrogen atoms and counteranions are not shown for clarity. Selected bond lengths (Å): Pt(1)−Pt(2) = 2.6453(3), Pt(2)−P(4) = 2.3056(19), Pt(1)−P(3) = 2.2835(16), Pt(1)−P(1) = 2.2906(17), Pt(2)−P(2) = 2.3108(15), Pt(1)−C(51) = 1.991(7), Pt(2)−C(61) = 1.989(7), C(51)−N(1) = 1.133(8), C(61)−N(2) = 1.151(9). Selected angles (deg): N(1)−C(51)−Pt(1) = 176.5(6), N(2)−C(61)−Pt(2) = 175.4(9), C(51)−Pt(1)−Pt(2) = 176.38(18), C(61)−Pt(2)−Pt(1) = 176.6(3), P(3)−Pt(1)−P(1) = 173.47(6), P(4)−Pt(2)−P(2) = 177.08(7).

compounds is demonstrated in two ways. First, the ν(Pt−Pt) modes are observed at 137 and 133 cm^{-1} for **M3** and **M4**, respectively, compared to 150 cm^{-1} for $Pt_2(dppm)_2Cl_2$.[23] The difference between the frequencies is the result of a predictable mass effect where the isocyanide ligand is heavier than the Cl atom.[24] Second, the typical dσdσ* band associated with the M_2 chromophore is observed for all model compounds (described further below).

The X-ray diffraction data for **M1**, **M3**, and **M4** were obtained, and the data confirmed their proposed structures (Figures 1−3, Table 1). On the basis of the Cambridge Crystallographic Data Base, crystallographically authenticated d^9−d^9 Pd_2 and Pt_2 complexes containing 2 axially substituted aryl or alkyl isocyanide ligands are rare (9 examples only),[25] but only two of them involve the $M_2(dppm)_2^{2+}$ fragment. One example is compound **M5** as depicted in Chart 3.[25a]

On the other hand, X-ray structures involving the $M_2(dppm)_2L_2^{2+}$ fragments, where L is anything but an isocyanide ligand, are more frequent in the literature.[26] The X-ray structures for **M1**, **M3**, and **M4** exhibit bond lengths and angles that are consistent with those from the literature.[25,26] The average dihedral PMMP angles are 41.2, 40.9, and 41.5° for **M1**, **M3**, and **M4**, respectively, which is typical for the $M_2(dppm)_2^{2+}$ skeleton. **M4** exhibits 2 crystallographically independent molecules, but the bond distances and angles do not significantly differ from each other.

M5 was obtained from the reaction between $Pd_2(dppm)_2Cl_2$ and 1-isocyano-2,6-dimethylbenzene,[25a] but a C−H bond activation occurred. In this work, **M2** was successfully prepared and used as a model compound. On the other hand, the 1-isocyano-4-isopropylbenzene isocyanide used for the synthesis of the corresponding model complex failed to provide pure samples. Since attempts to purify it failed, this ligand was not investigated further. For the Pt analogue (**M4**),

(23) Alves, O. L.; Vitorge, M.-C.; Sourisseau, C. *Nouv. J. Chem*. **1983**, *7*, 231.

(24) Herzberg, G. *Vibrational Spectra of Polyatomic Molecules*; Van Nostrand: New York, 1945; p.181. (b) Harvey, P. D.; Truong, K. D.; Aye, K. T.; Drouin, M.; Bandrauk, A. D. *Inorg. Chem.* **1994**, *33*, 2347.

(25) Rashidi, M.; Vittal, J. J.; Puddephatt, R. J. *J. Chem. Soc., Dalton Trans.* **1994**, 1283. (b) Tanase, T.; Nomura, T.; Yamamoto, Y.; Kobayashi, K. *J. Organomet. Chem.* **1991**, *410*, C25. (c) Tanase, T.; Nomura, T.; Fukushima, T.; Yamamoto, Y.; Kobayashi, K. *Inorg. Chem*. **1993**, *32*, 4578. (d) Cristofani, S.; Leoni, P.; Pasquali, M.; Eisentraeger, F.; Albinati, A. *Organometallics* **2000**, *19*, 4589. (e) Messbauer, B.; Meyer, H.; Walther, B.; Heeg, M. J.; Masqsudur Rahman, A. F. M.; Oliver, J. P. *Inorg. Chem.* **1983**, *22*, 272. (f) Goldberg, S. Z.; Eisenberg, R. *Inorg. Chem*. **1976**, *15*, 535. (g) Khan, Md. N. I.; King, C.; Wang, J.-C.; Wang, S.; Fackler, J. P. Jr. *Inorg. Chem.* **1989**, *28*, 4656.

(26) Selected references from the Cambridge Data Bank: (a) Hong, X.; Yip, H.-K.; Cheung, K.-K.; Che, C.-M. *J. Chem. Soc., Dalton Trans.* **1993**, 815. (b) Yip, H.-K.; Che, C.-M.; Peng, S.-M. *J. Chem. Soc., Dalton Trans.* **1993**, 179. (c) Maekawa, M.; Munakata, M.; Kuroda-Sowa, T.; Suenaga, Y. *Inorg. Chim. Acta* **1998**, *281*, 116. (d) Maekawa, M.; Munakata, M.; Kuroda-Sowa, T.; Suenaga, Y. *Anal. Sci*. **1998**, *14*, 447. (e) Besenyi, G.; Parkanyi, L.; Gacs-Baitz, E.; James, B. R. *Inorg. Chim. Acta* **2002**, *327*, 179. (f) Krafft, T. E.; Hejna, C. I.; Smith, J. S. *Inorg. Chem*. **1990**, *29*, 2682. (g) Henderson, W.; Nickelson, B. K.; Chung, D. C. *Acta Crystallogr. E* **2002**, *58*, m432. (h) Maekawa, M.; Munakata, M.; Kuroda-Sowa, T.; Suenaga, Y. *Polyhedron* **1998**, *17*, 3657. (i) Yip, J. H. K.; Wu, J.; Wong, K.-Y.; Ho, K. P.; Pun, C. S.-N.; Vittal, J. J. *Organometallics* **2002**, *21*, 5292.

Table 1. Crystal Data

	M1	M3	M4
empirical formula	$C_{60}H_{62}B_2F_8N_2P_4Pd_2$	$C_{60}H_{62}B_2F_8N_2P_4Pt_2$	$C_{70}H_{66}B_2F_8N_2P_4Pt_2$
fw	1321.42	1498.80	1622.93
cryst size (mm)	0.65 × 0.25 × 0.25	0.50 × 0.30 × 0.20	0.45 × 0.2 × 0.075
temp (K)	198(2)	293(2)	198(1)
cryst syst	orthorhombic	orthorhombic	orthorhombic
space group	$P2_12_12_1$	$P2_12_12_1$	*Pnma*
a (Å)	12.390(12)	12.536(8)	21.9667(12)
b (Å)	19.773(4)	19.930(6)	16.5006(9)
c (Å)	26.411(4)	26.5056(5)	36.265(2)
vol (Å^3)	6471(6)	6622(4)	13144.6(12)
Z	4	4	8
density$_{calcd}$ (Mg/m^3)	1.356	1.503	1.640
scan mode	ω	ω	ω and ϕ
F(000)	2680	2936	6384
abs coeff (mm^{-1})	5.920	9.191	4.416
θ range (deg)	3.94−69.96	3.90−70.00	1.54−25.00
limiting indices	$0 \le h \le 15$	$0 \le h \le 15$	$-25 \le h \le 26$
	$0 \le k \le 24$	$0 \le k \le 24$	$-19 \le k \le 18$
	$0 \le l \le 32$	$0 \le l \le 32$	$-43 \le l \le 42$
reflns collected	6358	6835	64795
ind reflns	6358	6835	22186
min/max trans. ratio	0.9895	0.2608	0.529
	0.8105	0.0912	
data/restraints/ params	6358/8/644	6835/420/629	22186/1/1594
GOF on F^2	0.980	1.083	1.040
final R[a] indices [$I>2\sigma(I)$]	R1 = 0.0686	R1 = 0.0595	R1 = 0.0263
	wR2 = 0.1762	wR2 = 0.1635	wR2 = 0.0650
R[a] indices (all data)	R1 = 0.1087	R1 = 0.0799	R1 = 0.0334
	wR2 = 0.2017	wR2 = 0.1772	wR2 = 0.0682
largest diff. peak and hole (e Å^{-3})	0.710	1.682	0.895
	−0.865	−1.391	−0.451

[a] $R1 = \sum||F_o| - |F_c||/\sum |F_o|$; $wR2 = (\sum[w(F_o^2 - F_c^2)^2]/\sum[F_o^4])^{1/2}$.

Chart 3

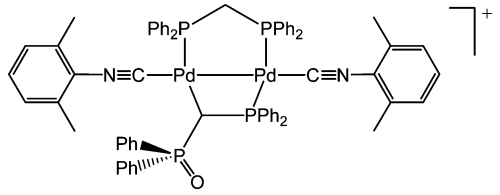

M5

since crystals suitable for X-ray analysis were obtained, **M4** was therefore treated as a model compound.

II. Polymers. (a) Syntheses and Characterization. The syntheses of **P1**−**P4** (Scheme 2) were carried out, as described for the model compounds, to generate orange materials exhibiting a single IR absorptions associated with coordinated isocyanides.

This single IR absorption suggests a long polymer chain for which a band at 2131 cm^{-1} (uncoordinated N≡C group) is not observed. This observation is obviously qualitative, and so, NMR was used to address this (^{1}H NMR integration for the PCH_2P (4H) signal vs dmb (18H) or C_6Me_4 (12H)). After the polymers were synthesized, they were dissolved in CD_3CN, and the ^{1}H NMR spectra were measured. On the basis of the integrations, the following $M_2(dppm)_2^{2+}$/bridging ligand ratios were obtained: **P1**, 1:0.99; **P2**, 1:0.97; **P3**, 1:1.00; **P4**, 1:0.99. The precision of the method depends on the precision of the integration (for example, the "worst" ratio (1:0.97) with PCH_2P (4H) = 4.00, dmb (18H) = 17.66). For comparison purposes, the ratios of **M1**−**M4** of $M_2(dppm)_2$ versus CNR are 1:1.89 (**M1**), 1:2.08 (**M2**), 1:2.01 (**M3**), and 1:2.00 (**M4**). Additional convincing proof for the formation of polymers is found in the behavior of the polymer during dissolution in acetonitrile. The polymers tend to swell or render the solution viscous prior to complete dissolution (pictures of **P4** are provided in the Supporting Information) and make stand-alone films. Smaller oligomers do not exhibit these properties. The vibrational activity of the ν(N≡C) modes (**P3** IR 2173, Raman 2183 cm^{-1}; **P4** IR 2148, Raman 2165 cm^{-1}) also indicates the presence of a local center of symmetry at the M_2-bonded fragment. The $\nu(M_2)$ vibrations (137 cm^{-1} for **P3** and 134 cm^{-1} for **P4**) and the $\lambda(d\sigma \rightarrow d\sigma^*)$ bands (detail provided below) are observed proving that the M−M bond remains intact. The absence of peaks attributable to oligomers or polymers in the MALDI-TOF spectra indicates the fragility of the polymers.

Scheme 2

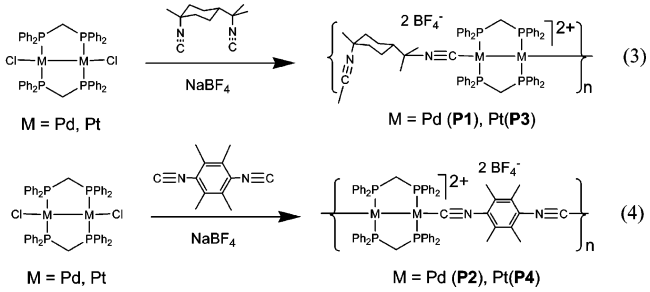

(b) Properties in the Solid State. All polymers are semicrystalline where two broad peaks characterize the powder diffraction films (XRD). A strong and broad diffraction peak at $2\theta \approx 8.5°$ and a weaker and broad one at ~21° are observed, indicating the presence of a somewhat

organized structure. On the other hand, the model compounds are crystalline. The semicrystalline properties for **P1**−**P4** contrast with the completely amorphous $\{Pd_2(dmb)_2(\mu\text{-diphos})^{2+}\}_n$ (diphos = $PPh_2(CH_2)_mPPh_2$, $m = 4-6$, Chart 1)[6a] polymers where only a large band at approximately 20 °C is observed. The flexibility of the $P(CH_2)_mP$ chain in the latter polymers may induce structural disorder.

Not surprisingly, the DSC traces indicate no T_g for **P1**−**P4** between −30 °C and the decomposition temperature (**P1**, 135 °C; **P2**, 225 °C; **P3**, 140 °C; **P4**, 270 °C). This result is consistent with the lack of T_g for the "more flexible" $\{Pd_2(dmb)_2(diphos)^{2+}\}_n$ (diphos = $Ph_2P(CH_2)_mPPh_2$, $m = 4-6$) and $\{Pd_2(diphos')_2(dmb)^{2+}\}_n$ (diphos′= $Ph_2P(CH_2)_mPPh_2$, $m = 2, 3$, Chart 1) polymers.[6b] The lack of T_g may be associated with limited motion of the polymer chain from the size of the $M_2(dppm)_2^{2+}$ fragment, the rigidity of the chain for the aryl diisocyanide, and the limitation in motion in the dmb ligand.

The thermal stability of the materials (**M1**−**M4** and **P1**−**P4**) was analyzed by TGA (Supporting Information), and the key features are listed below. The weight losses are sharp and the traces versus temperature exhibit plateaus. The full analysis was based on a comparison with the $M_2(dppm)_2Cl_2$ complexes where there are no CNR groups. The analyses show that the loss of BF_4 and isocyanides or the decomposition of isocyanides occurs at lower temperatures than that for the more robust $M_2(dppm)_2^{2+}$ fragments. In fact, losses of phenyl groups must occur to account for the weight losses at higher temperatures. In addition, the weight losses for Pt species occur at higher temperatures than those for the Pd analogues, which is consistent with the stronger Pt−L bond. Moreover, the alkyl isocyanide complexes and polymers are more temperature sensitive than the aryl analogues, consistent with favorable π-delocalization between the aryl group and the metal atom. **P4** turns out to be particularly robust being thermally stable up to 300 °C.

The **P1**−**P4** solids are electrically insulating with resistivities exceeding $10^8\ \Omega\ cm^{-1}$. Doping the solids with I_2 (1% in weight) did not decrease the resistivity, but rather, the color of the materials changed, presumably via an oxidative addition to the M−M bond.

(c) Properties in Solution. The M_n values were estimated by the T_1/NOE method which was fully described elsewhere[10] and applied several times by this group.[6a,27] A brief outline of the method is provided below.

The size of a molecule can be obtained from the Stokes−Einstein−Debye equation, assuming a spherical shape, if the correlation time, τ_c, is known ($\tau_c = V\eta_{visc}/kT$, η_{visc} = solvent viscosity, k = Boltzmann constant, T = temperature). To measure τ_c, one must know the spin−lattice relaxation time related to dipole−dipole interactions, T_1^{DD}, which is given by eq 5

$$1/T_1^{DD} = \sum (h^2\gamma_P{}^2\gamma_H{}^2/4\pi^4 r_{PH}{}^6)\,\tau_c \qquad (5)$$

(27) Plourde, P.; Gilbert, K.; Gagnon, J.; Harvey, P. D. *Organometallics* **2003**, *22*, 2862.

Chart 4

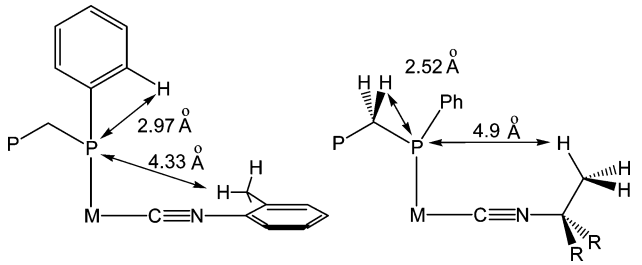

in the extreme narrowing limit,[28] where h is the Planck constant, γ is the gyromagnetic ratio for the interacting nuclei (^{31}P and ^1H in this case),[29] and r is the distance between the probe (here ^{31}P) and the nearest interacting nuclei (here ^1H). The T_1^{DD} data (here at 300 MHz ^1H) can be extracted from experimental T_1 and NOE measurements (nuclear Overhauser effect),[29b] according to eq 6

$$1/T_1^{DD} = \eta/(\eta_{max}T_1) \qquad (6)$$

where η = the fractional NOE constant, η_{max} = the maximum η value in the extreme narrowing limit (here $\eta_{max} = \gamma_H/2\gamma_P$), and T_1 is the experimental spin−lattice relaxation time.[30] The strategy is to compare the hydrodynamic volume of a known compound (ideally characterized from crystallography) to that of the unknown ones. One parameter that must be taken into account is that the standard molecule must be closely related to the sample molecule, not only in terms of structure, but also in terms of the charge due to solute−solvent interactions. In this work, the probe nuclei are the ^{31}P atoms because any tumbling of the molecule in solution is felt by these nuclei without major interference from unrelated motion, such as phenyl and methyl group rotations. By combining eqs 5 and 6 with the Stokes−Einstein−Debye equation, one obtains

$$\frac{T_1(sam)}{T_1(sta)} = \frac{\eta_{PH}(sam)}{\eta_{PH}(sta)}\,\frac{V(sta)}{V(sam)}\,\frac{\sum 1/r^6{}_{PH}(sta)}{\sum 1/r^6{}_{PH}(sam)} \qquad (7)$$

where "sam" and "sta" stand for sample and standard, respectively. This equation requires knowledge of the interatomic distances between the ^{31}P probe nucleus and the surrounding ^1H nuclei. The standard molecules are **M1**−**M4** for **P1**−**P4**, respectively. The greatest magnetic interactions between the P and H atoms are the P···H_2C and P···H(*o*-Ph) which exhibit the shortest distances based on average values extracted from X-ray and computer modeling (Chart 4). As the contribution to T_1 is proportional to $1/r^6_{PH}$, these interactions clearly dominate the relaxation processes.

(28) T_1 decreases with the field (H_0) indicating the extreme narrowing limit.
(29) Drago, R. S. *Physical Methods for Chemists*, 2nd ed.; Saunders College Publishing: New York, 1992. (b) Wehrli, F. W.; Wirthlin, T. *Interpretation of Carbon-13 NMR Spectra*; Heyden: London, 1980.
(30) The contribution from chemical shift anisotropy, quadrupolar, electron paramagnetic, chemical exchange, and spin−rotation processes are negligible. Indeed, the complex does not exhibit quadrupolar nuclei (except for ^{14}N, which exhibits a very small quadrupolar constant, 2×10^{-26} cm^2)[28] nor are they paramagnetic. The fwhm (full-width-at-half-maximum) was not strongly temperature dependent between 20 and 40 °C.

Chart 5

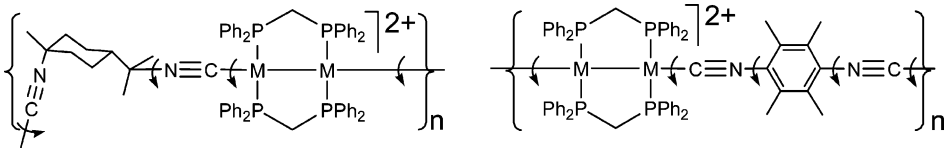

Table 2. T_1/ NOE Analyses and Comparison with Light Scattering Data

	T_1 (s)	η_{PH}	V (Å^3)[a]	V(sam)/V(sta)	n[b]	M_n	M_w	n
M1	3.88	*c*	1245					
P1	1.25	*c*	1200				2600 ± 800	1.9
M2	2.39	0.73	1306					
P2	1.45	0.93	1208	2.10	2.3	3000	5230 ± 300	3.9
M3	3.54	0.46	1245					
P3	1.11	0.34	1200	2.36	2.4	3500	6650 ± 800	4.3
M4	3.22	0.60	1378					
P4	1.77	0.83	1208	2.52	2.9	3800	14700 ± 300	9.7

[a] Computed using PC Model software. [b] $n = [V(\text{sam})_{\text{exptl}}/V(\text{sta})_{\text{exptl}}][V(\text{sta})_{\text{calcd}}/V(\text{sam})_{\text{calcd}}]$. [c] Not measured.

With standard molecules where the $M_2(\text{dppm})_2$ moiety remains the same, the term $[\sum 1/r^6_{PH}(\text{sam})]/[\sum 1/r^6_{PH}(\text{sta})]$ becomes unity, and the V(sta)/V(sam) ratio can easily be extracted. By computing the gas phase volume of standards, the experimentally evaluated V(sta)/V(sam) ratio leads to the number of units, n, in the tumbling polymers or oligomers using the following equation $n = [V(\text{sam})_{\text{exptl}}/V(\text{sta})_{\text{exptl}}][V(\text{sta})_{\text{calcd}}/V(\text{sam})_{\text{calcd}}]$.

Data and analysis are presented in Table 2, and they are compared to that of light scattering data (M_w). Both methodologies reveal the presence of small oligomers and the same trend (**P4** > **P3** > **P2**, ignoring the experimental uncertainties), but significant discrepancies are noticed for the rigid rod polymers. For **P3**, the T_1/NOE and light scattering data indicate n values of 2.4 and 4.3, respectively. For **P4**, this difference is more important (2.9 vs 9.7).[6a] $N(T_1/\text{NOE})/n(\text{viscosity})$ ratios of ∼1/3 to ∼1/4 were previously observed for other related d^9-d^9 Pd−Pd-containing oligomers (Chart 1) and are the result of the presence of single bonds in the oligomer chain. This allows extra motion which contributes to the relaxation (Chart 5).[6a]

This discrepancy becomes more important when one considers that the oligomers exhibit a linear shape, while the Stokes−Einstein−Debye equation assumes a spherical shape. NOE data were not collected for **M1** and **P1** as similar conclusions were anticipated.

Attempts to evaluate M_v from viscosity measurements were also made. While the data reproducibly indicated the presence of short oligomers on the basis of the measured times, the estimation of M_v is difficult because of the nature of the oligomers. There is no standard that would be appropriate to apply to this methodology. However, the delay times for **P1**−**P4** in acetonitrile are as follow: **P1** 1 (0.4%), 12 (1%), and 33 (2%); **P2** 13 (0.3%), and 15 (0.5%); **P3** 6 (0.4%), 10 (0.8%), and 14 (1.2%); and **P4** 70 (0.4%), and 149 s (0.9%). When 0.4% is used as a common concentration (averaging the data for **P2**), the delay times vary as Pd < Pt and dmb < CNC_6Me_4NC. Assuming that the delay times are proportional to M_v, these data are perfectly consistent with the data extracted with the light scattering method. The data are also consistent with the larger degree of dissociation of the Pd−L bond than that of the Pt−L bond and the fact that π-delocalization in the M−C≡N-aryl fragment occurs (as concluded with the TGA findings). The dimension of the oligomers is best described by the light scattering data in this work (Table 2).

Chart 6

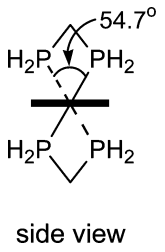

side view

All in all, **P1**−**P4** are unquestionably oligomers in solution, while they are polymers in the solid state. It is reasonable to assume that the acetonitrile solvent molecule occupies the vacant site at the axial position of the dissociated M_2 fragments.

III. Molecular Orbital Analysis. Theoretical computations on "gas phase" models such as the $Pd_2(H_2PCH_2PH_2)_2(C{\equiv}NR)_2^{2+}$ (R = Me, Ph) complexes for **M1** and **M2** were performed to address the nature of the frontier MOs. Geometry optimizations on both compounds exhibit the twisted $Pd_2(\text{diphos})_2$ fragment (dihedral PPdPdP angle 54.7°) and axially placed isocyanide groups along the M−M bond. The phenyl groups in $Pd_2(H_2PCH_2PH_2)_2(C{\equiv}NPh)_2^{2+}$ adopt a symmetric conformation where the planes are placed perpendicular to the $CH_2{\cdots}CH_2$ axis (Chart 6). This result is consistent with the X-ray data for **M4** where the undistorted isocyanide ligand (Figure 3) also adopts this geometry.

The bond distances listed in the figure captions (Figures 4 and 5) compare reasonably to that of the X-ray data (Figures 1−3, ref 26). The largest discrepancy is the Pd−P bond where the computed value is 0.069 Å longer than the experimental averaged value.

The computed frontier MOs for $Pd_2(H_2PCH_2PH_2)_2(C{\equiv}NMe)_2^{2+}$ (Figure 4) exhibit the $d\sigma$ (HOMO) and $d\sigma^*$ (LUMO) typical for the presence of the d^9-d^9 M−M bond.[31,6a] On the other hand, the frontier MOs for $Pd_2(H_2PCH_2PH_2)_2(C{\equiv}NPh)_2^{2+}$ (Figure 5) exhibit two series of degenerate $\pi^*-d\pi^*$ (HOMO and HOMO-1) and intraligand π(Ph) MOs (HOMO-2 and HOMO-3). HOMO and HOMO-1 indicate the presence of π-interactions between the $Pd_2(H_2PCH_2PH_2)_2^{2+}$ fragment and the aryl isocyanides and are consistent with the observed electronic communication in

(31) Harvey, P. D.; Murtaza, Z. *Inorg. Chem.* **1993**, *32*, 4721−4729.

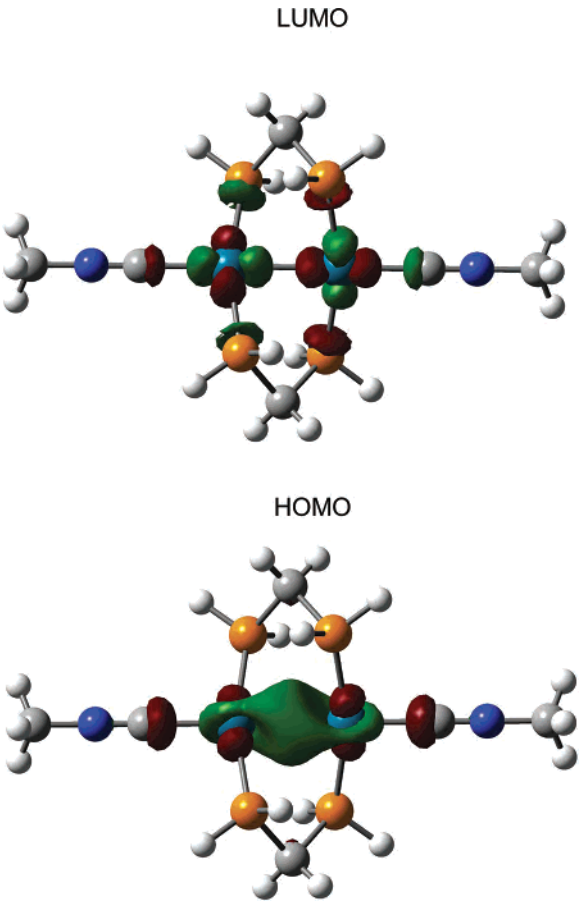

Figure 4. MO drawings for the frontier orbitals for $Pd_2(H_2PCH_2PH_2)_2(CNMe)_2^{2+}$. The optimized geometry exhibits the following structural parameters: $d(Pd_2) = 2.650$ Å, $d(PdP) = 2.369$ Å, $d(PdC) = 2.123$ Å, $d(C{\equiv}N) = 1.166$ Å, $\angle(PPdP) = 164.3°$, $\angle(PdPdC) = 180.0°$, $\angle(PdCN) = 180.0°$, $\angle(PdPdP) = 82.2°$, and $\angle(PPdC) = 97.9°$; PPdPdP torsion angle = 54.7°.

the $[FcC{\equiv}C{-}Pt_2(dppm)_2{-}C{\equiv}CFc]^{+2}$ cation and the observed enhanced thermal stability of the aryl isocyanide complexes (with respect to alkyl isocyanide) discussed above. The HOMO-4 and LUMO are the dσ and dσ* MO, respectively. The main feature for these calculations is that virtual intraligand and $\pi^*{-}d\pi^*$ states are present in the frontier MOs and must be taken into account prior to UV−vis and luminescence analyses.

IV. Electronic Spectra and Photophysics. (a) Absorption Spectra. The absorption spectra of **M1**−**M4** and **P1**−**P4** exhibit low-energy bands that are narrow and sharpen upon cooling of the solutions to 77 K (see Figure 6 for examples) which suggest the presence of d$\sigma \rightarrow$ dσ* electronic transitions associated with $d^9{-}d^9$ M_2-bonded species. These bands generally exhibit low energies and high intensities ($\epsilon > 10\,000$ M^{-1} cm^{-1}), and they are often narrow ($2000 <$ fwhm < 4000 cm^{-1} at room temperature).[33] The most striking piece of evidence for such a band in the UV−vis spectra is the high sensitivity of the λ_{max} and fwhm to temperature. When the samples are cooled, either in the solid state or in solution, the d$\sigma \rightarrow$ dσ* bands experience a

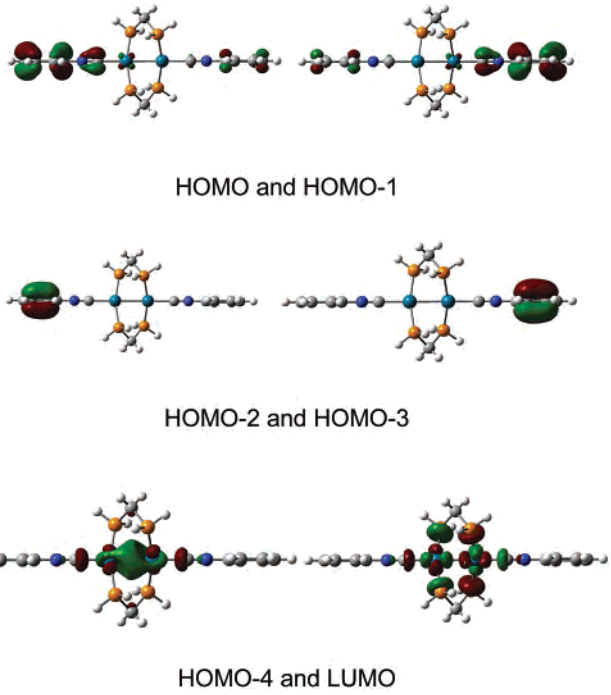

Figure 5. MO drawings for the frontier orbitals for $Pd_2(H_2PCH_2PH_2)_2(CNPh)_2^{2+}$. The optimized geometry exhibits the following structural parameters: $d(Pd_2) = 2.647$ Å, $d(PdP) = 2.369$ Å, $d(PdC) = 2.116$ Å, $d(C{\equiv}N) = 1.170$ Å, $\angle(PPdP) = 164.4°$, $\angle(PdPdC) = 179.9°$, $\angle(PdCN) = 180.0°$, $\angle(PdPdP) = 82.2°$, and $\angle(PPdC) = 97.8°$; PPdPdPd torsion angle = 54.7°.

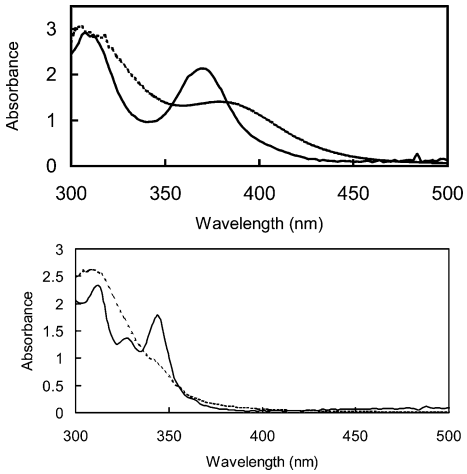

Figure 6. UV−vis spectra of **P2** (up) and **P4** (down) in butyronitrile at 298 (—) and 77 K (- -).

significant blue shift and decrease in fwhm. This well-known phenomenon is the result of lower-energy "hot bands" of vibronic origin, which disappear upon cooling.[33] The presence or absence of such hot bands depends on the vibrational frequency of the Franck−Condon active modes in the electronic transitions. For d$\sigma \rightarrow$ dσ* transitions, this mode is $\nu(M_2)$, which is generally of low frequency, leading to significant "hot band" contributions in the d$\sigma \rightarrow$ dσ* spectral envelope. For MLCT (metal-to-ligand-charge-transfer) or d−d transitions, higher frequency Franck−Condon active modes are generally present, such as intraligand and M−L stretches. Because of their greater energy gap, the higher vibrational levels are not heavily populated. Sourisseau and co-workers used resonance Raman to demonstrate the d$\sigma \rightarrow$ dσ*

(32) Yip, J. H. K.; Wu, J.; Wong, K.-Y.; Ho, K. P.; Pun, S.-N.; Vittal, J. J. *Organometallics* **2002**, *21*, 5292.
(33) Miskowski, V. M.; Smith, T. P.; Loehr, T. M.; Gray, H. B. *J. Am. Chem. Soc.* **1985**, *107*, 7925.

Table 3. UV−vis Data for **M1**−**M4** and **P1**−**P4**

	298 K (in butyronitrile)				77 K (in butyronitrile)		
	λ(max)[a] (nm)	ν(max)[b] (cm^{-1})	ϵ[c] ($M^{-1}\,cm^{-1}$)	fwhm[d] (cm^{-1})	λ(max)[a] (nm)	ν(max)[b] (cm^{-1})	fwhm[c] (cm^{-1})
M1	378	26460	10300	3410	366	27320	3100
P1	372	26880	8570	4500	366	27320	2830
M2	378	26460	16850	3370	364	27470	
P2	380	26320	12000	4570	370	27030	2640
M3	334	29940	3680	2740	328	30490	2150
P3	338	29590	4350	2670	332	30120	2440
M4	342	29240	11900	1980	340	29410	1680
P4	344	29070	15000	2280	344	29070	1160

[a] The uncertainty is ±1 nm. [b] The uncertainty is ±70 cm^{-1}. [c] The uncertainty is ±5%. [d] The uncertainty is ±150 cm^{-1}.

assignment of the lowest-energy absorption band at ~420 nm for $Pd_2(dppm)_2Cl_2$.[34] Indeed, this band is seen at about 380 and 340 nm for the Pd- and Pt-containing materials, respectively. Table 3 shows the magnitude and the important decrease in fwhm with the decrease in temperature of these spin-allowed bands and corroborates the $d\sigma \rightarrow d\sigma^*$ assignment. The absorptivity data are found between 10 000 and 15 500 $M^{-1}\,cm^{-1}$, as expected, but the data for **M3** and **P3** (about 4000 $M^{-1}\,cm^{-1}$) are unusual but not shocking.

(b) Luminescence. Unstructured emission bands are observed in the 635−750 nm range with excitation spectra superimposing the absorption spectra (Table 4, Figure 7 as an example). The large Stokes shifts (>10 000 cm^{-1}) and τ_e (μs time scale for the Pt species) suggest phosphorescence, and the lack of vibronic resolution rules out the intraligand $\pi-\pi^*$ excited state as the luminescent state, on the basis of comparison with the ligands themselves. Consequently, we assign the luminescent band to a triplet $d\sigma-d\sigma^*$ transition. The emission spectra of $Pt_2(dppm)_2(CNC_6Me_2H_3)_2^{2+}$ were also investigated to address the effect of substitution on the aromatic on the luminescence. In PrCN at 77 K, the λ_{emi} is 680 nm, which is similar to M4 (673 nm, Table 4). Therefore, it has almost no effect.

Because of dissociation of the **P1**−**P4** polymers in solution, oligomers capped with $NCCH_3$ ligands must be considered as well. To this end, the known $M_2(dppm)_2(NCCH_3)_2^{2+}$ complexes (M = Pd, Pt) were also investigated. The $Pd_2(dppm)_2(NCCH_3)_2^{2+}$ complex is very weakly luminescent under the same experimental conditions as for **M1**−**M4** and **P1**−**P4**, to the extent that one cannot measure λ_{emi} in the solid state. $Pt_2(dppm)_2(NCCH_3)_2^{2+}$ is also very weakly luminescent, but not as much as the former Pd-analogue, and λ_{emi} could be measured in all cases. The λ_{emi} data for the $M_2(dppm)_2(NCCH_3)_2^{2+}$ complexes are very similar to that of **M3**, **M4**, **P3**, and **P4** (Table 4). This behavior probably reflects on the similarity in axial ligands between cyanide and isocyanide. Therefore, one cannot distinguish between the photophysics from these two ligands in this work. However, since the bis-acetonitrile model complexes are very weakly luminescent, the luminescence depicted in the oligomers must result mainly from isocyanide-containing fragments.

The comparison of λ_{emi} between **M2** and **P2** and between **M4** and **P4** exhibits large red shifts of the emission bands in the oligomers in solution at 77 K, suggesting that π-delocalization plays a role in the excited-state properties. This is supported by the comparison between λ_{emi} for **M1** and **P1**, as well as for **M3** and **P3**, where only small red shifts are observed. In the solid state, no accurate conclusion could be made as the emission band turned out to be broad.

Intrachain excitonic processes are occasionally encountered for AgCNR- and CuCNR-containing polymers in solution.[35] These processes involve reversible energy transfer, either in the singlet or triplet states, along a series of identical chromophores after one of them has been photoexcited. After an undetermined amount of time (generally within the time scale of relaxation of a single chromophore), the polymer relaxes by emitting a photon. The observed luminescence is completely different from that of a single unit where the emission lifetime decay traces are nonexponential, the emitted light is depolarized, and the time-resolved spectra exhibit an "infinite" number of emission bands with different delay times. In this work, despite the use of delocalized systems (M−C≡N−aryl), excitonic processes were not observed, suggesting that the photophysical process seems, for the moment, to be specific to AgCNR- and CuCNR-containing polymers.

(c) Photophysical Properties. Because of the weak intensity of the signal, the emission lifetimes, τ_e, could not be determined accurately in the solid state at both 298 and 77 K. However, solution data were acquired, and the key features are as follows. First, the τ_e data for Pd-containing materials are significantly shorter than those of the Pt analogues (by about 2 orders of magnitude, Table 4). This is consistent with the fact that the emission intensities for the Pt materials are larger than those of the Pd materials. Second, the τ_e data are not greatly influenced by polymerization.

The first feature appears to be unusual when one considers the larger spin−orbit coupling effect on τ_e (τ_e decreases as the atomic number increases). However, the nanosecond time scale has been encountered for all mixed-ligand d^9-d^9 Pd_2 materials. For example, the $Pd_2(dmb)_2X_2$ (X = Cl, Br),[31] $Pd_2(dmb)_2(PPh_3)_2^{2+}$,[6a] $\{Pd_2(dmb)_2(diphos)^{2+}\}_n$ (diphos = $Ph_2P(CH_2)_mPPh_2$ where m = 4, 5, 6; $Ph_2C{\equiv}CPPh_2$),[6a] $\{Pd_2(dmb)_2(diphos')^{2+}\}_n$ (diphos′ = $Ph_2P(CH_2)_mPPh_2$ where m = 2, 3) materials[6a] exhibit τ_e values of of 71, 177, 2.8, 1.9, 2.7, 2.2, 2.4, 1.9, and 1.5 ns, respectively in PrCN at 77 K. The particularly short lifetimes in the $Pd_2(dmb)_2X_2$ (X = Cl, Br) complexes were assigned to a facile photoinduced Pd−Pd cleavage and the photolability of the ligands.[31] For the Pt analogues, the Pt−L bonds are much less labile, as indirectly observed in the greater thermal stability of the Pt−CNR bonds (TGA) and the longer oligomers in solution (light scattering data above).

The second feature is interesting as excited-state deactivations associated to molecular vibrations and motions in solution are the same for the model compounds and for the

(34) Alves, O. L.; Vitorge, M.-C.; Sourrisseau, C. *Nouv. J. Chim.* **1983**, *7*, 231.

(35) Harvey, P. D.; Fournier, É. ACS Books, in press, 2005.

Table 4. Emission Data for **M1-M4** and **P1-M4** in the Solid State at 77 and 298 and in Solution at 77 K

	solid state		solution (77 K)		
	λ_{emi} (nm) at 77 K	λ_{emi} (nm) at 298 K	λ_{emi} (nm)	ν_{emi} (cm^{-1})	τ_e
$Pd_2(dppm)_2(NCCH_3)_2^{2+}$	*a*	*a*	740	13500	*b*
M1	730	683	730	13700	*b*
P1	*a*	*a*	750	13300	6.2 ± 0.4 ns
M2	*a*	*a*	635	15700	4.5 ± 0.4 ns
P2	727	700	720	13900	3.7 ± 0.1 ns
$Pt_2(dppm)_2(NCCH_3)_2^{2+}$	735	734	675	14800	*b*
M3	741	738	676	14800	3.2 ± 0.2 μs
P3	714	712	680	14700	4.1 ± 0.7 μs
M4	750	745	673	14900	3.1 ± 0.6 μs
P4	732	727	715	14000	3.1 ± 0.3 μs

[a] Too weak to be detected. [b] Too weak to be accurately measured.

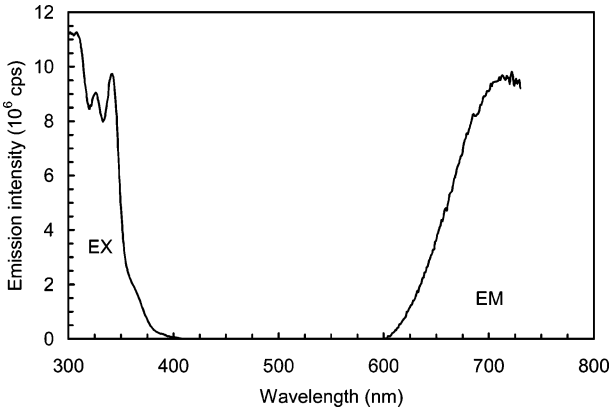

Figure 7. Emission (EM, $\lambda_{ex} = 380$ nm) and excitation (EX, $\lambda_{em} = 610$ nm) spectra of **P4**, $\{[Pt_2(dppm)_2(CNC_6Me_4NC)](BF_4)_2\}_n$, in PrCN at 77 K.

oligomers. The size of the oligomers does not affect these processes as the τ_e of the oligomers and of the model complexes are approximately the same. Therefore, no autoquenching of the excited states occurs.

Conclusion

This study provides a better understanding of coordination/organometallic polymers, particularly with respect to their nature in solution and in the solid state. While clear evidence for polymers in the solid state is observed, 2−10 unit long oligomers are observed in solution. The length is function of the metal and of the ligand. The thermal stability is governed by the weakest bond (M−CNR), common to all diisocyanide-containing polymers. In this series, the most stable material is found for M = Pt and R = aryl (**P4**).

Reported M−M-containing polymers are scarce, and this work shows that the presence of the M−M bonds in the backbone is felt in the photophysics of these weakly luminescent materials, in both the solid state and in solution. However, while π-delocalization occurs in the aryl-containing materials, no intrachain excitonic behavior is noted here, which is surprising at this moment.

Acknowledgment. P.D.H. thanks the Natural Sciences and Engineering Research Council (NSERC) for funding. Dr. Frédéric Brisach is acknowledged for the measurements of the emission and excitation bands and emission lifetimes of the Pd-containing materials at 77 K.

Supporting Information Available: Table providing TGA analyses of **M1**−**M4** and **P1**−**P4** and the $M_2(dppm)_2Cl_2$ complexes, pictures of **P4** in the solid state and dissolved in a minimum amount of CH_3CN showing the swelling, General experimental details for X-ray crystallography, crystal data and structure refinement, atomic coordinates and equivalent isotropic displacement parameters, bond lengths and angles, anisotropic displacement parameters, hydrogen coordinates and isotropic displacement parameters, and torsion angles for **M1**, **M3**, and **M4** (98 pages). Crystallographic data files in CIF format. This material is available free of charge via the Internet at http://pubs.acs.org.

IC0509480